Energy 167 (2019) 921–938

Contents lists available at ScienceDirect

Energy

journal homepage: www.elsevier.com/locate/energy

Transient cooling and operational performance of the cryogenic part in reverse Brayton air refrigerator

Shanju Yang [a], Bao Fu [b], Yu Hou [c], Shuangtao Chen [c], Zhiguo Li [a], Shaojin Wang [a, d, *]

[a] Northwest A&F University, College of Mechanical and Electronic Engineering, Yangling, Shaanxi 712100, China
[b] Institute of Plasma Physics, Chinese Academy of Sciences, Hefei 230031, China
[c] State Key Laboratory of Multiphase Flow in Power Engineering, Xi'an Jiaotong University, Xi'an 710049, China
[d] Department of Biological Systems Engineering, Washington State University, 213 L.J. Smith Hall, Pullman, WA 99164-6120, USA

ARTICLE INFO

Article history:
Received 25 July 2018
Received in revised form
16 October 2018
Accepted 5 November 2018
Available online 12 November 2018

Keywords:
Reverse Brayton air refrigerator
Transient cooling model
Dynamic matching
Regenerator
Experiment
Energy efficiency

ABSTRACT

Accurate calculation of the transient cooling performance is crucial for the operation and control of a reverse Brayton refrigerator. Components of the refrigerator have complex working characteristics individually and interact each other mutually. To solve the problem easily, the turboexpander matching characteristics were usually ignored and relations among components were simplified. In this study, a cryogenic reverse Brayton air refrigerator equipped with gas bearing turboexpander and plate-fin heat regenerator was presented. The ultimate refrigerating temperature was proposed through analysis. The transient cooling characteristics of the cryogenic part in refrigerator were resolved into the turboexpander matching performance and the regenerator transient cooling characteristics. The regenerator was simulated through numerical heat transfer and computational fluid dynamics by considering the axial conduction and cold loss. The matching model was improved by adopting a significant method of constant rotating speed. Using the dual non-steady time steps, a transient cooling model of the cryogenic part was explored via C++ code, and verified by experiment. Through the model, the refrigerator cooling performances were evaluated under different operation modes, and the energy utilization efficiency was determined. It can be used to evaluate the operation strategy of refrigerators and help to promote energy efficiency.

1. Introduction

As an important cryogenic machine, the reverse Brayton refrigerator is applied in many fields, such as gas separation [1] and liquefaction [2], telescope [3] and liquid hydrogen storage [4] in space, environment simulation [5], nuclear fusion engineering [6], high temperature superconducting [7], road conditioner [8], heat pump [9], and food processing [10]. The turboexpander and heat regenerator are two main devices of the cryogenic reverse Brayton refrigerator. Expanding the gas through a turboexpander is an effective way to get low temperatures. Due to regeneration, the refrigerator could operate under low operation pressures in practice. Thus, equipped with efficient turboexpander and compact regenerator, the refrigerator could achieve high efficiency, large cooling capacity, light weight, small dimension, and high operation reliability. With the gas bearing turboexpander, the refrigerator has special advantages of long life, negligible vibration, oil free, and wide range of refrigeration temperature [11].

Due to the low refrigerating temperature, great thermal capacity of cryogenic components, and the regeneration effect, a cryogenic reverse Brayton refrigerator may undergo a complex and long cooling period before reaching refrigerating temperature. For example, the turboexpander outlet temperature in a Neon reverse Brayton refrigerator decreased from 290 K to 80 K in 250 min [7]. The transient cooling characteristics, which include the cooling time, cooling patterns, the lowest refrigerating temperature, and economic costs, are very important for the optimization and control of a refrigerator. Thus, many experiments have been conducted to study the transient characteristics of the reverse Brayton refrigerator and the similar turbo-based refrigeration systems. Hirai et al. [7] developed a reverse Brayton cryocooler for HTS (High Temperature Superconducting) applications. They tested the transient cooling performance and measured the cooling capacity through an

* Corresponding author. Northwest A&F University, College of Mechanical and Electronic Engineering, Yangling, Shaanxi 712100, China.
E-mail address: shaojinwang@nwsuaf.edu.cn (S. Wang).

https://doi.org/10.1016/j.energy.2018.11.016
0360-5442/

Nomenclature

A_{min}	area of nozzle throat (m^2)
c_p	specific heat (J K^{-1} kg^{-1})
f	friction factor
G	mass velocity (kg m^{-2} s^{-1})
h	heat transfer coefficient (W m^{-2} K^{-1})
j	heat transfer factor
k_E	adiabatic exponent in expander
n_Z	polytropic exponent in nozzle
p_{0E}	expander inlet pressure (Pa)
p_{2E}	expander outlet pressure (Pa)
Pr	Prandtl number
w_C	compression work (W kg^{-1})
W_E	expansion work (W)
W_F	brake work of blower (W)
q_0	cooling capacity (W kg^{-1})
R	gas constant of air (J Kg^{-1} K^{-1})
Re	Reynolds number
S	volume heat source (W m^{-3})
St	Stanton number
T	temperature (K)
T_{0E}	expander inlet temperature (K)
T_{2E}	expander outlet temperature (K)
u	velocity (m s^{-1})
V	volume (m^3)
Z_{0E}	compression factor in expander

Greek

ε_C	compressor pressure ratio
ε_E	expander expansion ratio
$\Delta\varepsilon$	relative pressure drop
η_C	compressor isentropic efficiency
η_E	expander isentropic efficiency
η_M	machinal efficiency
η_R	regenerator effectiveness
τ	time (s)
ρ	density (kg m^{-3})
λ	thermal conductivity (W m^{-1} K^{-1})
$\dot{\Phi}$	volume heat source (W m^{-3})

electric heater. Then they developed a volumetrically smaller turbo-compressor, which made the refrigerator more compact and efficient [12]. The design and test were clarified and the analysis was less. Davis et al. [13] presented the mechanical and transient cooling performance of a large size turboexpander compressor for LNG (Liquefied Natural Gas) plant through several tests. Dolan et al. [14] tested steady and transient performances of a reverse Brayton cryocooler for space application, which involved system thermal performances of cooling loads, refrigerating temperatures, power levels and rejection temperatures. Deserranno et al. [3] performed optimization of a Brayton cryocooler for ZBO (Zero Boil Off) liquid hydrogen storage in space and tested the compressors and turboalternator under different operating conditions. The COP (Coefficient of Performance) of the cryocooler reached as high as 23% of the Carnot cycle. Yang et al. studied cooling characteristics of a reverse Brayton refrigerator with expansion works of consumption [15] and recovery [16]. They established a reverse Brayton refrigerator with turboexpander compressor and tested the transient coupling performance during the cooling process [16]. Although transient cooling performances were described in these studies, the inherent cooling characteristics and connected relations among components were not presented.

Besides experiments, the transient simulation is an efficient way to determine performances of the reverse Brayton refrigerator, and could provide a basis for its optimization and control. To accurately calculate the transient performance of the refrigerator is quite difficult. The refrigerator mainly includes the compressor, turboexpander, heat regenerator, after cooler, and cold load, which all affect the refrigerator. They have complex working characteristics individually and interact each other mutually. Thus, many working processes and component characteristics are simplified for the sake of calculation. Wang et al. [17] and Cai et al. [18] established mathematical models of the air refrigerator's components and calculated the cooling process of the refrigerator. In the models, the steady-state heat transfer calculation was adopted for the regenerator but great error was obtained. As mentioned in Refs. [17,18], the analysis method of unitary flow loss for turboexpander simplified the matching characteristics but caused larger calculation errors. Ahmadi et al. [19] conducted ecological and thermal optimization of a cryogenic refrigerator system using the genetic algorithm. In the thermal analysis, the regenerator effectiveness was discussed in details and the expansion performance was simplified. They developed multi-objective optimization algorithms based on NSGA-II algorithm to optimize the cryogenic refrigerator [20] and a four-temperature-level absorption refrigerator [21]. Thermodynamic analysis of optimization was then conducted for the irreversible absorption refrigerator [22]. Zhan et al. [23] conducted dynamic simulation of a single nitrogen expansion cycle, in which all the component modes were developed. The calculation of regenerator was described in detail but the axial conduction of regenerator was ignored. The matching performance of turboexpander were also simplified for the convenience of solving the problem.

The commercial simulators and models based on math software packages are also commonly used to study the transient cooling performance of refrigerators. Fazlollahi et al. conducted economic costs and exergy analysis for several optimized cryogenic systems [24]. Then they used the Aspen HYSYS software to study steady-state and transient models of natural gas liquefaction processes [25]. They also used the HYSYS to optimize two natural gas liquefaction processes and identified the rate-limiting components during load variations [26]. He et al. [27] developed a dynamic model to investigate the dynamic behaviors of a small-scale LNG plant. McCormick [28] performed a design and test of a reverse Brayton cryocooler and carried out performance prediction for the 35 K cooler. Shin et al. [29] developed a control-oriented system model for a boil-off gas re-liquefaction plant and designed its effective control structure. But the connection between the expander and heat exchanger was not presented. Bradu et al. [30] illustrated a simulator PROCOS (PROcess and COntrol Simulator) for a helium system, and the simulator was satisfactory for achieving accurate predictions of the system behaviors. These simulators could provide relatively accurate results, but detailed descriptions of the calculation principle and process were not presented. Also, few studies have been focused on the detailed transient cooling characteristics of the reverse Brayton cycle. Additionally, the matching characteristics of the turboexpander and mutual relations between the turboexpander and regenerator were usually simplified and ignored, which affected the prediction accuracy. Thus, it is urgent to establish an accurate and efficient transient

cooling model with detailed descriptions of the refrigerator.

In this study, steady-state parameters analysis of the refrigerator was carried out firstly, and the ultimate refrigerating temperature of the refrigerator was newly defined. Based on the transient analysis, the cooling characteristics of the cryogenic part in refrigerator were resolved into the transient expansion performance of the turboexpander and the transient heat transfer characteristics of the regenerator. The regenerator model was solved through methods of numerical heat transfer and computational fluid dynamics. The turboexpander matching model was modified and improved by adopting a significant method known as the constant rotating speed. Different from exist models, a method of dual non-steady time steps was newly proposed to connect transient characteristics of the turboexpander to the regenerator, and the transient cooling model was explored via Visual C++ code. Theoretical calculations were conducted to qualitatively clarify impacts of components on the refrigerator with the ultimate refrigerating temperature. Exergy analysis was performed to help validating the rationality of the transient model and to provide a basis for the optimization. The results of the transient cooling model were compared with experimental data. Transient cooling performances (cooling speed, cooling pattern, refrigerating temperature, economic costs) under varied operation modes and control strategies were evaluated quantitatively through the model. The energy utilization efficiency and mutual relations between the turboexpander and regenerator were clarified. The objectives of this study were to analyze the transient cooling performance of the cryogenic part in reverse Brayton refrigerator accurately, provide a basis for the design and optimization of refrigerators, and allow for establishing the operation and control strategies.

2. Description and analysis of the refrigerator

2.1. Description of the refrigerator

The working process and *T-s* diagram of the reverse Brayton air refrigerator in this study are illustrated in Fig. 1. This refrigerator was composed of three parts: the compression, the brake and the refrigeration. The compression part consisted of a compressor, a freezing dryer, an adsorption dryer and a buffer. It provided 0.087 kg s^{-1} clean air at 1.000 MPa. The refrigeration part mainly consisted of an electric proportional valve, an expander, a vacuum pump, and a cold box, which included a plate-fin heat exchanger, a cooling load and cryogenic pipes. The vacuum degree of the cold box can reach 0.01 Pa. The expander (cold side of the turboexpander) was placed verticality in the cold box. The hot side of the turboexpander belonged to the brake part, which was similar with the one shown in Ref. [15]. An electric proportional valve and a chock valve were used to have the brake pressure at certain values. A cooler was applied to absorb the heat from the compression process of the blower. The thermodynamic process of the refrigerator is presented in Fig. 1 (b). The main design parameters of the turboexpander and regenerator are listed in Table 1.

Table 1
Main design parameters of the turboexpander and regenerator.

Items	Turboexpander values	Regenerator values
Inlet pressure (abs. MPa)	0.500	0.510
Outlet pressure (abs. MPa)	0.110	0.100
Mass flow rate (kg s^{-1})	0.032	0.032
Isentropic efficiency or effectiveness (%)	57.8	93.0

In the test apparatus, all the platinum resistance thermometers were calibrated and the maximum uncertainty was ±0.1 K in the range of 320.0 K–55.0 K. The full-scale uncertainty of the pressure gauge was ±0.25% in the range of 0.000 MPa–1.000 MPa. The full-scale uncertainty of the flow rate was ±1.5% in the range of 0.003 kg s^{-1} to 0.060 kg s^{-1}. The rotating speed was measured by an eddy current sensor, and the uncertainty was ±1 rpm.

2.2. Target parameter analysis

To establish an integrated cooling model of the refrigerator, the transient performance of each component should be solved, and

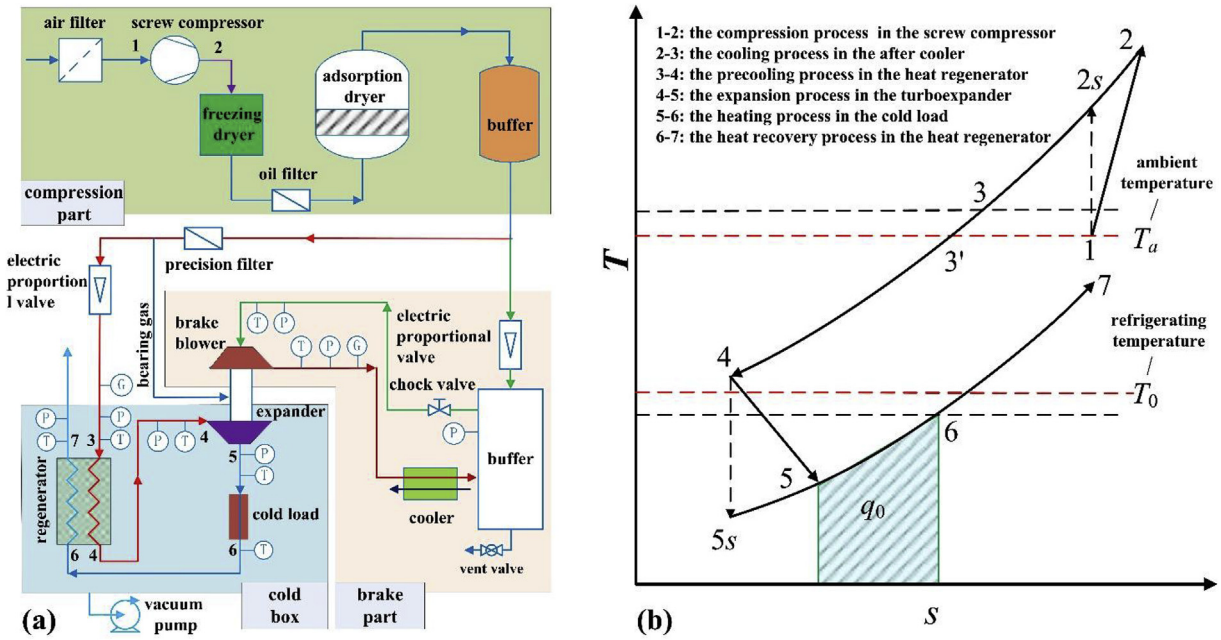

Fig. 1. Schematic view and *T-s* diagram of the reverse Brayton air refrigerator.

corresponding mathematical models should be established. The models were also required to be correlated according to mutual relations of the components, which could be extremely difficult and many simplifying assumptions have to be introduced. In this paper, steady-state parameters analysis and calculation of the refrigerator were also carried out since they reflect final results of the transient process. The steady calculations could provide some necessary theoretical verification and corroborations for the transient cooling model.

In the steady cyclic analysis, the following hypotheses were adopted:

(1) The air in the system was ideal gas, and the ambient pressure was atmospheric pressure.
(2) The heat transfer process in heat exchanger was isobaric, and the pressure drops in heat exchangers and pipelines were reduced to flow resistance uniformly.
(3) The temperature difference for heat transfer in the cold device was considered in the refrigerating temperature for simplification.
(4) The cold loss of the system was reduced to the load of the cold device but was no longer considered in the cycle analysis.

The cooling capacity of the refrigerator q_0 and the compression work of the compressor w_C are defined as [1]. The COP of the refrigerator is the ratio of q_0 to w_C. According to the above hypotheses, the COP can be given as:

$$\mathrm{COP} = \frac{q_0}{w_C} = \frac{c_p(T_2 - T_1)}{c_p(T_6 - T_5)} = \frac{T_0 - [(T_a + \Delta T_1)(1-\eta_R) + T_0\eta_R]\left[1 - \eta_E\left(1 - \varepsilon_E^{1/k-1}\right)\right]}{T_a\left(\varepsilon_C^{1-1/k} - 1\right)\Big/\eta_C} \tag{1}$$

where $\Delta T_1 = T_a - T_3$, $\eta_R = \frac{T_3 - T_4}{T_3 - T_0}$, $T_5 = T_4[1 - \eta_E(1 - \varepsilon_E^{1/k-1})]$, and $\varepsilon_E = \varepsilon_C(1 - \Delta\varepsilon)$.

When COP = 0, T_m represents the lowest temperature that the refrigerator could reach.

$$T_m = T_0 = \frac{(1-\eta_R)\left[1 - \eta_E\left(1 - \varepsilon_E^{1/k-1}\right)\right]}{1 - \eta_R\left[1 - \eta_E\left(1 - \varepsilon_E^{1/k-1}\right)\right]}(T_a + \Delta T_1) \tag{2}$$

The COP is one of the main performance indexes of refrigerators. In practice, the refrigerator may run under various conditions for a long time and the refrigerating temperature is usually lower than the design value due to the change of refrigeration demand. Therefore, it is necessary to analyze the ultimate refrigeration ability of the refrigerator. The outlet temperature of expander represents the lowest one of the cycle. When the expander outlet temperature is equal to the refrigerating one, the cooling capacity produced by the expander is totally used to pre-cool the inlet air of expander. By this time, the expander outlet temperature is defined as the ultimate refrigerating one while the refrigerator COP is zero. It represents the lowest refrigerating temperature in which the refrigerator could reach under certain operation parameters. In an experiment, the lowest temperature that can be reached without a cold load is the ultimate refrigerating temperature. Therefore, the ultimate refrigerating temperature connects the steady state and transient one, and could be target parameters to help analyzing the refrigerator cooling performance.

2.3. Transient analysis

As shown in Fig. 1, in the cryogenic refrigerator, the screw compressor and after cooler run under room temperature and relatively stable operational conditions. The heat regenerator belongs to the cryogenic part, and there is large temperature difference between its cold and hot ends. It experiences the whole temperature change from the ambient temperature to a low temperature. The expander also belongs to the cryogenic part, and its inlet temperature and rotating speed vary greatly in the cooling process [7,9,16]. Superadding variations of the expansion ratio, these make the change of expander characteristics very complicated. Therefore, transient characteristics of the turboexpander and regenerator should be the main content for studying the refrigerator transient cooling characteristics.

For a practical refrigerator, despite the working characteristics of the regenerator and expander, there are some other factors that affect the transient cooling and operational performances, such as the cold loss and thermal capacity of the cooling load, heat regenerator, expander, and pipes. Influences of them should be analyzed according to features of the refrigerator working process and the thermal properties of components. The progress of air flowing through the regenerator, cooling load and turboexpander in the cold box is shown in Fig. 2.

The turboexpander and heat regenerator were placed in the cold box of high vacuum and covered by multi-screens reflecting layers. Therefore, the cold loss through radiation was little and could be ignored for simplification. The regenerator was made of aluminum, with a total thermal capacitivity of 51567.3 J K^{-1}. The cryogenic pipes in the cold box were brass, with a total thermal capacitivity of 97.8 J K^{-1}. The cold end of the turboexpander (expander) was using stainless steel, with a total thermal capacitivity of 786.5 J K^{-1}. Compared with the heat regenerator, the thermal capacitivity of

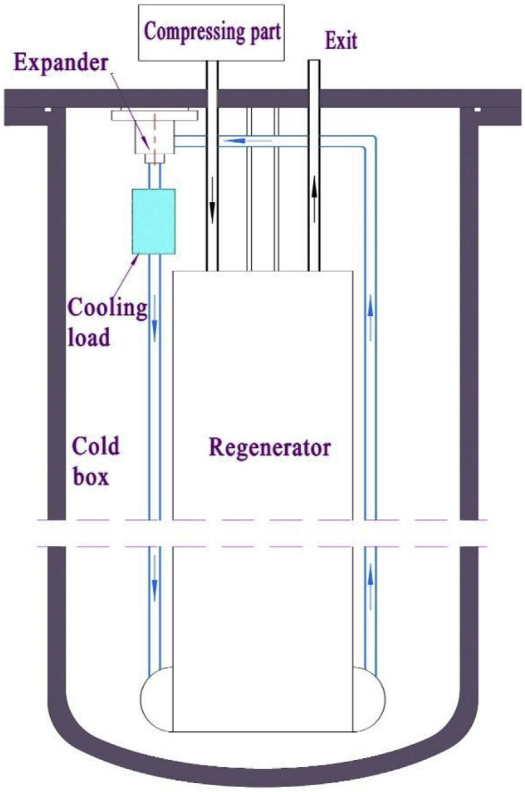

Fig. 2. The progress of air flowing through the cold box.

cryogenic pipes and expander were quite small and could be ignored. In the refrigerator, the cooling capacity was measured through the electric heater. Therefore, the cooling characteristics of the refrigerator were expressed with no-load. The transient cooling characteristics of the cold load, mainly determined by its physical properties, volume and weight, were relatively simple and could be easily obtained when related parameters were settled.

Figs. 1 and 2 show that temperatures of the system were the ambient one at the begging. After the screw compressor was started, the temperature in the expander outlet was decreasing by adiabatic expansion. The low temperature gas flowed through the cooling load and cooled the expander inlet gas in the heat regenerator through transient heat transfer. Repeating this, the refrigerator was cooling down. In the cooling down process, operation parameters of turboexpander can be recognized as the quasi steady state. The turboexpander became stable quickly when the operating parameters were fixed [1,7,16]. Thus, the transient expansion performance was the off-design matching behavior of the turboexpander. The transient cooling characteristics of the cryogenic part in refrigerator could be resolved into the dynamic matching performance of the turboexpander and the transient heat transfer characteristics of heat regenerator. Then the transient cooling model of the cryogenic part in reverse Brayton air refrigerator could be established. To obtain the complete transient model, the working characteristics of regenerator and turboexpander should be determined and all related models should be established.

3. Transient cooling model

3.1. Heat regenerator model

The heat regenerator is a plate-fin heat exchanger. According to methods of numerical heat transfer and computational fluid dynamics, a transient computational model for plate-fin heat exchanger was proposed. To acquire relatively accurate results, cold loss through heat conduction, influences of the axial conduction of parting plates, and thermal capacity of the heat exchanger were comprehensively considered in the model. Discrete equations of the model were deduced by control volume integral method. Several following classical assumptions were adopted for simplification, which represented the thermal change features and could help solve the model easily [31]:

(1) The flow inside the heat exchanger was in one dimension.
(2) The acceleration pressure drop in the momentum equation was negligible.
(3) The energy dissipation from friction was not added as heat to the fluid.
(4) The fluid was distributed evenly in channels of the heat exchanger.

These assumptions could also be verified by numerical simulations for the three-dimensional plate-fin heat exchanger based on Ansys Fluent. A rigorous simulation should be based on conservation laws of mass, momentum and energy. With these assumptions, only the energy conservation is required to be considered [31,32]. Heat is transferred between adjacent channels directly through the separating plates and by conduction through the fins. The energy equations for the fluid and parting plate could be solved with methods of numerical heat transfer. Temperature descriptions of fluids and parting plates could be obtained. The schematic view of the plate-fin heat exchanger is shown in Fig. 3. The main structure parameters of the regenerator are listed in Table 2.

The correlations of heat transfer and pressure drop used for the plate-fin heat exchanger are listed as below [32]:

$$f = 8.12\left(a_f/D_h\right)^{-0.41}\left(s_f/H_f\right)^{-0.02}\mathrm{Re}^{-0.74} \quad \mathrm{Re} \le \mathrm{Re}^* \tag{3}$$

$$j = 0.53\left(a_f/D_h\right)^{-0.15}\left(s_f/H_f\right)^{-0.14}\mathrm{Re}^{-0.5} \quad \mathrm{Re} \le \mathrm{Re}^* \tag{4}$$

$$f = 1.12\left(a_f/D_h\right)^{-0.65}\left(\delta_f/D_h\right)^{0.17}\mathrm{Re}^{-0.36} \quad \mathrm{Re} \ge \mathrm{Re}^* + 1000 \tag{5}$$

$$j = 0.21\left(a_f/D_h\right)^{-0.24}\left(\delta_f/D_h\right)^{0.02}\mathrm{Re}^{-0.4} \quad \mathrm{Re} > \mathrm{Re}^* + 1000 \tag{6}$$

where, a_f is the cutting length, $\mathrm{R}_\mathrm{e}^* = 257\left(\frac{a_f}{s_f}\right)^{1.23}\left(\frac{\delta_f}{a_f}\right)^{0.58}D_h\left[\delta_f + 1.328\left(\frac{\mathrm{R_e}}{a_f D_h}\right)^{-0.5}\right]^{-1}$, $D_h = \frac{2(s_f-\delta_f)H_f}{(s_f+H_f)+H_f\delta_f/a_f}$.

Table 2
Main structure parameters of the plate-fin heat exchanger.

Parameters	H_f	s_f	δ_f	x	y	δ_w	a_f
Value/mm	9.5	1.2	0.2	1.0	9.3	1.2	10

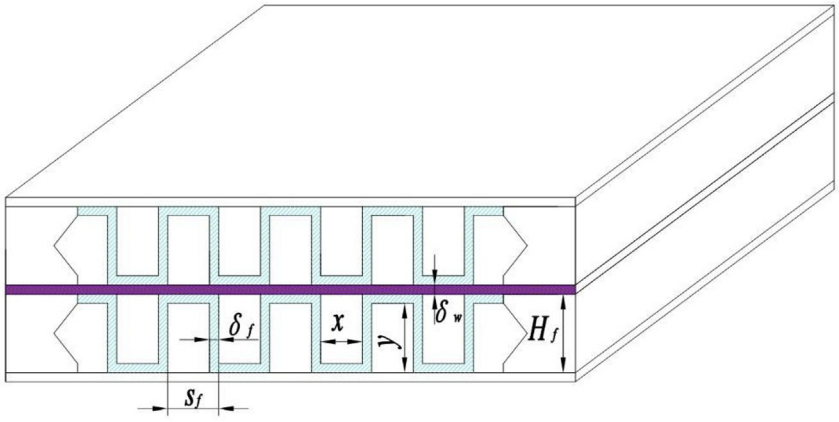

Fig. 3. The structure schematic view of the plate-fin heat exchanger.

After calculating the factors of heat transfer and pressure drop, the Stanton number *St* could be obtained.

$$\mathrm{St} = j \Big/ \mathrm{Pr}^{2/3} \tag{7}$$

where $\mathrm{Pr} = c_p\mu/\lambda$.

Then, the convective heat transfer coefficient and pressure drop in the plate-fin heat exchanger could be calculated as below [32]:

$$h = \frac{c_p\mu}{\mathrm{Pr}^{2/3}}\frac{1}{D_h} j\mathrm{Re} = \mathrm{St}c_pG \tag{8}$$

$$\Delta p = 4f\frac{l}{D_h}\frac{G^2}{2\rho} \tag{9}$$

where Δp is the pressure drop (Pa) and l is the length of flow channel (m).

If considering all the fluids and parting plates in calculation, the computation load would be heavy, resulting in long solution time. The cryogenic heat exchanger is the two-fluid plate-fin heat exchanger, and parting plates are between hot and cold fluids, as shown in Fig. 3. To accelerate the computation, only two fluids (a cold fluid and a hot fluid) and a plate need to be conducted instead of all the fluids and plates. Since there are 8 sets for the regenerator, the simplification is reasonable.

Finite volume method was used to disperse the calculation area. The discrete equations derived by the finite volume method have advantages of conservation properties, and clear physical meanings. A uniform grid was used to divide the cold area, hot area and the parting plate. The node was set up as the internal node. The compute grids of the regenerator in the numerical model are shown in Fig. 4. The self-adaptive mesh method was adopted to improve the accuracy of the calculation.

Heat transfer within the parting plates and fins can be analyzed by the transient heat conduction equation, as shown in Eq. (10).

$$\frac{\partial T}{\partial \tau} = \frac{\lambda}{\rho c}\frac{\partial^2 T}{\partial^2 x} + \frac{\Phi^{\bullet}}{\rho c} \tag{10}$$

The energy transfer inside the plates is shown in Fig. 5. The energy transfer includes the heat conduction inside the plates and the heat convection between the plates and the fluid. The energy transmitted through heat convection is presented in the differential equation in the form of source term.

The control volume integral method was adopted, and Eq. (10) was integrated in the time interval $\Delta\tau$ and the volume shown in Fig. 5. Integration of the unsteady item is:

$$\int_x^{x+\Delta x}\int_\tau^{\tau+\Delta\tau}\frac{\partial T}{\partial \tau}d\tau dx = \int_x^{x+\Delta x}\left(T^{\tau+\Delta\tau} - T^{\tau}\right)dx = \left(T_{w,i}^{j+1} - T_{w,i}^{j}\right)\Delta x \tag{11}$$

To integrate the diffusion term, we have the first derivative change explicitly with time, and obtain the first derivative value of the interface by piecewise linear method.

$$\begin{aligned}\int_\tau^{\tau+\Delta\tau}\int_x^{x+\Delta x}\frac{\partial^2 T}{\partial^2 x}dxd\tau &= \int_\tau^{\tau+\Delta\tau}\left[\left(\frac{\partial T}{\partial x}\right)_{x+\Delta x} - \left(\frac{\partial T}{\partial x}\right)_x\right]d\tau \\ = \left[\left(\frac{\partial T}{\partial x}\right)_{x+\Delta x}^{\tau} - \left(\frac{\partial T}{\partial x}\right)_x^{\tau}\right]\Delta\tau &= \frac{T_{w,i+1}^{j} - 2T_{w,i}^{j} + T_{w,i-1}^{j}}{\Delta x}\Delta\tau\end{aligned} \tag{12}$$

The heat transfer between the plate and the fluid in the interface was converted into the volume heat source of the entire plate control volume, and the total parameter method was applied. The source term was integrated with time explicit:

$$\int_\tau^{\tau+\Delta\tau}\int_x^{x+\Delta x}\dot{\Phi}_i\, dxd\tau = \frac{1}{V_w}\left[h_{h,i}^{j}b_{h,i}\left(T_{h,i}^{j} - T_{w,i}^{j}\right) + h_{c,i}^{j}b_{c,i}\left(T_{c,i}^{j} - T_{w,i}^{j}\right)\times\right]\Delta x\Delta\tau \tag{13}$$

where V_w is the volume of a single control body (m^3), $h_{h,i}$ is the convective heat transfer coefficient at hot side ($W\cdot m^{-2}\cdot K^{-1}$), $b_{h,i}$ is the convective heat transfer area at hot side (m^2), $h_{c,i}$ is the

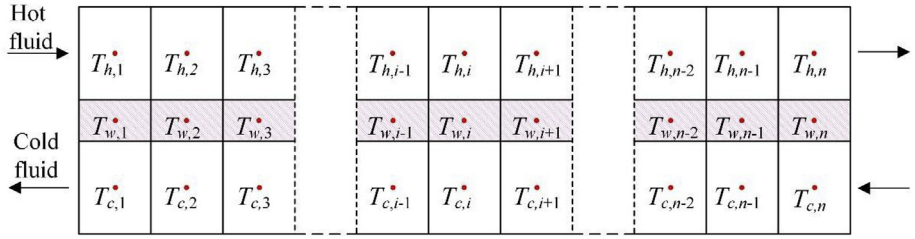

Fig. 4. The compute grid of the regenerator.

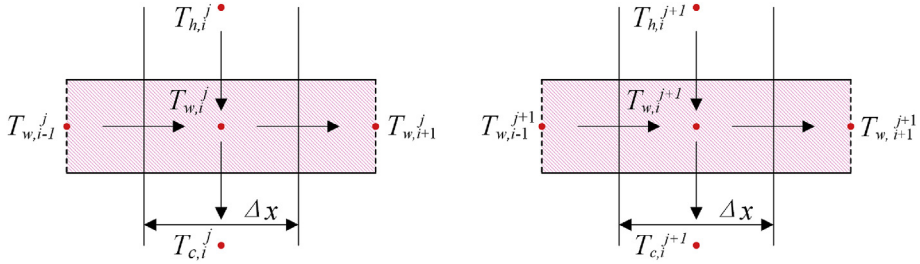

Fig. 5. Energy flow within the plate.

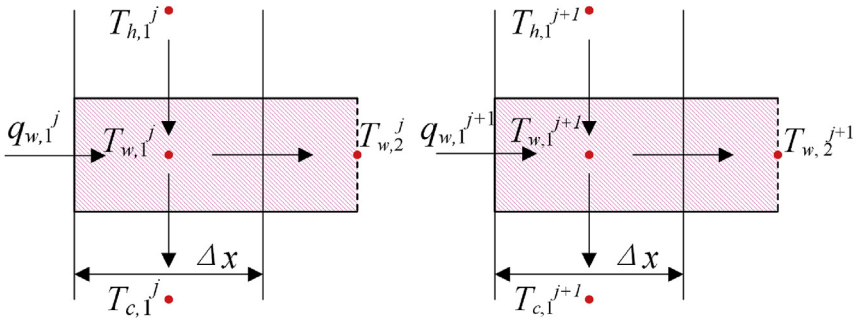

Fig. 6. Energy flow at the hot end of plate.

convective heat transfer coefficient at cold side ($W \cdot m^{-2} \cdot K^{-1}$), and $b_{c,i}$ is the convective heat transfer area at cold side (m^2).

Substituting Eqs. (11)–(13) into Eq. (10), the following equation is obtained:

$$\frac{\rho_w c_{p,w}\left(T_{w,i}^{\ j+1} - T_{w,i}^{j}\right)}{\Delta\tau} = \frac{\lambda_w\left(T_{w,i+1}^{j} - 2T_{w,i}^{j} + T_{w,i-1}^{j}\right)}{\Delta x^2} + \frac{1}{V_w}\left[h_{h,i}^{j} b_{h,i}\left(T_{h,i}^{j} - T_{w,i}^{j}\right) + h_{c,i}^{j} b_{c,i}\left(T_{c,i}^{j} - T_{w,i}^{j}\right)\right] \tag{14}$$

where ρ_w is the density of parting plate (kg m^{-3}); $\lambda_w$is the thermal conductivity of parting plate (W m^{-1} K^{-1}); $i = 2,3, \ldots, n\text{-}1$; $j = 1,2, \ldots, m\text{-}1$.

As shown in Eq. (14), the diffusion term is of central difference, which could transmit the disturbance downstream and upstream uniformly. It conforms to the physical characteristics of diffusion. Thus, it is an ideal discretization schemes, and has a 2-order intercept precision.

The energy transfer at the hot end of the plat is shown in Fig. 6. The energy transfer condition at the hot end is different from that of the internal control volume. Since it's the first control volume of the plate, there is heat coming from the external environment through heat conduction. Thus, the upstream boundary is set as heat flux (e.g. the second boundary condition). It also reflects the influence of cold loss on the heat regenerator. The heat transfer equation is shown in Eq. (15). The energy transfer at the cold end of the partition is like that of the hot end.

$$\frac{\rho_w c_{p,w}\left(T_{w,1}^{j+1} - T_{w,1}^{j}\right)}{\Delta\tau} = \frac{\lambda_w\left(-T_{w,1}^{j} + T_{w,2}^{j}\right)}{\Delta x^2} + \frac{q_{w,1}^{j}}{\Delta x} + \frac{1}{V_w}\left[h_{h,1}^{j} b_{h,1}\left(T_{h,1}^{j} - T_{w,1}^{j}\right) + h_{c,1}^{j} b_{c,1}\left(T_{c,1}^{j} - T_{w,1}^{j}\right)\right] \tag{15}$$

The heat transfer of the fluid in cold and hot channels is the transient heat convection, and the non-steady convection-diffusion heat transfer equation is:

$$\frac{\partial \rho T}{\partial \tau} + \frac{\partial \rho u T}{\partial x} = \frac{\partial}{\partial x}\left(\frac{\lambda}{c}\frac{\partial T}{\partial x}\right) + S \tag{16}$$

As shown in Eq. (16), the heat transfer contains the convection of flow and the diffusion term caused by heat conduction. According to the physical characteristics of the air, the Peclet Number (Pe) is high when the velocity is low. By this time, the influence of heat conduction or diffusion could be ignored. Therefore, the diffusion effect was omitted when calculating.

The control volume of the hot fluid is shown in Fig. 7. The energy transfer in the control volume of moment j and j+1 is given. The energy flowing into and out of the control body is transferred through convective flow. The energy exchanged between the fluid and the plate can be regarded as a generalized source term. When the numerical solution is performed, the temporal and spatial discretization of the transient item, the convection term and the source term should be conducted, respectively.

The unsteady term is dispersed as:

$$\int_x^{x+\Delta x}\int_\tau^{\tau+\Delta\tau} \frac{\partial \rho T}{\partial \tau} d\tau dx = \int_x^{x+\Delta x}\left[(\rho T)^{\tau+\Delta\tau} - (\rho T)^{\tau}\right] dx = \left[(\rho T)_{h,i}^{j+1} - (\rho T)_{h,i}^{j}\right]\Delta x \tag{17}$$

Other than the mathematical point of view, the convection term is the most difficult derivative term to disperse in the physical process, mainly because it has a strong directionality. The first-order windward format has the characteristics of migration, absolute stability and conservation. However, it has only the first order truncated precision. To overcome the disadvantages and maintain its advantages, the second order windward format is adopted. Using the time explicit, the convection terms are dispersed by the second order windward formats:

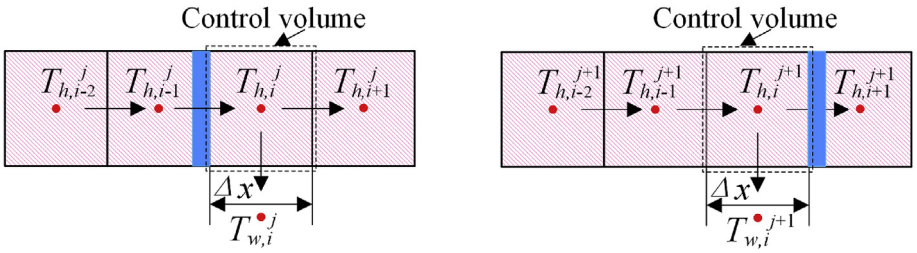

Fig. 7. Energy flow within the hot fluid.

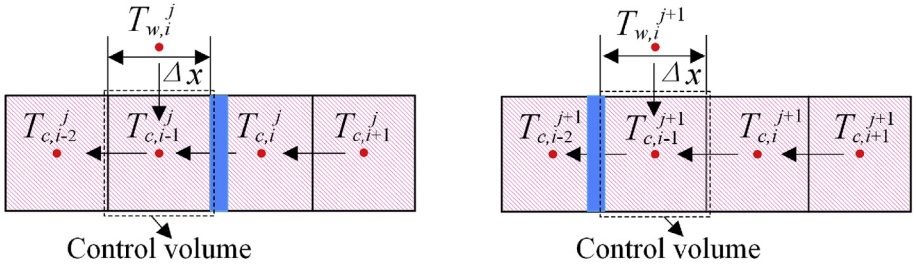

Fig. 8. Energy flow within the cold fluid.

$$\int_{\tau}^{\tau+\Delta\tau}\int_{x}^{x+\Delta x}\frac{\partial \rho uT}{\partial x}dxd\tau=\frac{\left[3(\rho uT)_{h,i}^{j}-4(\rho uT)_{h,i-1}^{j}+(\rho uT)_{h,i-2}^{j}\right]\Delta\tau}{2} \tag{18}$$

The convection heat transfer between the hot fluid and the plate is treated as source term:

$$S_{h,i}=\frac{q_{h,i}}{c_{p,h}a_h\Delta x}=\frac{b_{h,i}h_{h,i}(T_{w,i}-T_{h,i})}{c_{p,h}a_h\Delta x} \tag{19}$$

where $q_{h,i}$ is the convection heat transfer at the ith control volume (W); $c_{p,h}$ is the specific heat capacity of air in the hot channels ($\mathrm{J\cdot kg^{-1}\cdot K^{-1}}$).

The source term is integrated with the time explicit:

$$\begin{aligned}\int_{\tau}^{\tau+\Delta\tau}\int_{x}^{x+\Delta x}Sdxd\tau&=\int_{\tau}^{\tau+\Delta\tau}\int_{x}^{x+\Delta x}\frac{b_ih_{h,i}(T_{w,i}-T_{h,i})}{c_{p,h}a_h\Delta x}dxd\tau\\&=\frac{b_{h,i}h_{h,i}^{j}\left(T_{w,i}^{j}-T_{h,i}^{j}\right)\Delta\tau}{c_{p,h}a_h}\end{aligned} \tag{20}$$

The convection term is integrated with the second order windward, and the whole convection heat transfer equation can be arranged as:

$$\begin{aligned}\frac{a_hc_{p,h}\left(\rho_{h,i}^{j+1}T_{h,i}^{j+1}-T_{h,i}^{j}\rho_{h,i}^{j}\right)}{\Delta\tau}&=-\frac{a_hc_{p,h}\left(3\rho_{h,i}^{j}u_{h,i}^{j}T_{h,i}^{j}-4T_{h,i-1}^{j}\rho_{h,i-1}^{j}u_{h,i-1}^{j}+T_{h,i-2}^{j}\rho_{h,i-2}^{j}u_{h,i-2}^{j}\right)}{2\Delta x}\\&+\frac{h_{h,i}^{j}b_{h,i}\left(T_{w,i}^{j}-T_{h,i}^{j}\right)}{\Delta x}\end{aligned} \tag{21}$$

As shown in Eq. (21), the mass flow rate can be adopted instead of the velocity comprehensively and rigorously.

$$\begin{aligned}\frac{a_hc_{p,h}\left(\rho_{h,i}^{j+1}T_{h,i}^{j+1}-T_{h,i}^{j}\rho_{h,i}^{j}\right)}{\Delta\tau}&=-\frac{m^jc_{p,h}\left(3T_{h,i}^{j}-4T_{h,i-1}^{j}+T_{h,i-2}^{j}\right)}{2\Delta x}\\&+\frac{h_{h,i}^{j}b_{h,i}\left(T_{w,i}^{j}-T_{h,i}^{j}\right)}{\Delta x}\end{aligned} \tag{22}$$

where m^j is the mass flow rate ($\mathrm{kg\cdot s^{-1}}$); $i=3,\ldots,n$; $j=1,2,\ldots,m$-1.

Because the second order windward belongs to the three-point format, the second control volume at the entrance of the hot fluid is calculated using the first-order windward format.

$$\begin{aligned}\frac{a_hc_{p,h}\left(\rho_{h,2}^{j+1}T_{h,2}^{j+1}-T_{h,2}^{j}\rho_{h,2}^{j}\right)}{\Delta\tau}&=-\frac{m^jc_{p,h}\left(T_{h,2}^{j}-T_{h,1}^{j}\right)}{2\Delta x}\\&+\frac{h_{h,2}^{j}b_{h,2}\left(T_{w,2}^{j}-T_{h,2}^{j}\right)}{\Delta x}\end{aligned} \tag{23}$$

The control volume of the cold fluid is shown in Fig. 8. The energy transfer in the control body of moment j and j+1 is given. The flow and heat transfer conditions of the cold and hot fluids are similar. The convection heat transfer discrete equations of the cold side have the same form as those of the hot side.

$$\begin{aligned}\frac{a_cc_{p,c}\left(\rho_{c,i}^{j+1}T_{c,i}^{j+1}-T_{c,i}^{j}\rho_{c,i}^{j}\right)}{\Delta\tau}&=-\frac{m^jc_{p,c}\left(3T_{c,i}^{j}-4T_{c,i+1}^{j}+T_{c,i+2}^{j}\right)}{2\Delta x}\\&+\frac{h_{c,i}^{j}b_{c,i}\left(T_{w,i}^{j}-T_{c,i}^{j}\right)}{\Delta x}\end{aligned} \tag{24}$$

$$\begin{aligned}&\frac{a_cc_{p,c}\left(\rho_{c,n-1}^{j+1}T_{c,n-1}^{j+1}-T_{c,n-1}^{j}\rho_{c,n-1}^{j}\right)}{\Delta\tau}\\&=-\frac{m^jc_{p,c}\left(T_{c,n-1}^{j}-T_{c,n}^{j}\right)}{2\Delta x}+\frac{h_{c,n-1}^{j}b_{c,n-1}\left(T_{w,n-1}^{j}-T_{c,n-1}^{j}\right)}{\Delta x}\end{aligned} \tag{25}$$

where $c_{p,c}$is the specific heat capacity of air in the cold channels ($\mathrm{j.kg^{-1}\ k^{-1}}$); $i=3,4,\ldots,n$-1; $j=1,2,\ldots,m$-1.

3.2. Turboexpander model

Since the matching characteristics influence the thermal performance of the turboexpander greatly, a matching model is necessary for calculating transient cooling characteristics of the cryogenic part in refrigerator. Matching characteristics of the turboexpander with brake blower were studied and the mathematical model was established in Ref. [15]. When air is expanded in the expander, the enthalpy may drop with energy output. To keep the

balance, the output energy should be absorbed completely by the brake blower. The equilibrium parameters between the expander and brake blower consist of the working power and rotating speed. The expander drives the blower and is coaxial, which means they have the same rotating speed. The compression work nearly equals to the expansion work. Then the relation between operation parameters of the expander and the brake blower could be obtained as the following [15]:

$$p_{0F}T_{0E} = M\frac{p_{0E}}{(u_1/c_s)^3}\left(1-\varepsilon_E^{1-k_E/k_E}\right)^{0.5}\eta_E T_{0F} \tag{26}$$

where $M = \frac{\pi A_{\min} n_d D_{1E}^3}{169.7(1+\beta)\mu Q_d D_{2F}^2}\left[\frac{n_z-1}{Z_{0E}}\left(\frac{2}{n_z+1}\right)^{\frac{n_z+1}{(n_z-1)}}\right]^{0.5}$, where p_{0F} is the brake pressure of blower (Pa), T_{0F} is the inlet temperature of blower (K), D_{2F} is the diameter of blower wheel (m), $n_d$is the design speed of blower (r min^{-1}), Q_d is the design inlet flow rate of blower (m^3 min^{-1}), β is the friction and windage loss factor of blower, and μ is the slip factor of blower.

The characteristic ratio of expander u_1/c_s is defined as [33].

$$\frac{u_1}{c_s} = \frac{\pi D_{1E} n}{60\sqrt{2h_{Es}}} = \frac{\pi D_{1E}}{60\sqrt{2\frac{k_E}{k_E-1}R\left(1-\varepsilon_E^{\frac{1-k_E}{k_E}}\right)}}\frac{n}{\sqrt{T_{0E}}} \tag{27}$$

where D_{1E} is the diameter of expansion wheel (m).

As shown in Eq. (26), M and T_{0F} are approximated constants for a certain turboexpander. Thus, the matching characteristics are focused on the operation parameters of expander, expansion characteristics (performance curves) and the brake pressure. Among these, the essential factor is to obtain the expander performance curves. Simulations on the expander were performed for this purpose.

In the present study, when using ANSYS CFX to simulate the thermal performance of expander, the SST (Shear Stress Transport) k-ω model was applied instead of the k-ε model [15]. With the SST model, the expansion performances could be simulated more accurately [16,34]. The real air was chosen as working fluid in the simulation. The inlet boundary conditions were the mass flow rate and static temperature, and the outlet boundary condition was the static pressure. The solid surfaces were considered to be no-slip and adiabatic. The simulated performance curves for the expander were presented in Fig. 9. The expansion ratio compared with characteristic ratio are two decisive similarity criterions to determine the expander efficiency [15,33]. There exited an optimal characteristic ratio that made the expansion efficiency maximum, and the performance curves were somewhat different under varied expansion ratios. It can be seen from Eq. (27) and Fig. 9 that, any variations of the rotating speed, expander inlet temperature and expansion ratio may lead to the change of characteristics ratio, thus the change of efficiency.

The matching model of turboexpander with brake blower could be established, as shown in Fig. 10. For a given brake pressure, the stable rotating speed, characteristic ratio and efficiency could be obtained through computation. For a given expander characteristic ratio, the required brake pressure versus varied operation parameters of expander could also be calculated through the model. The operation methods of the feed back control (optimal characteristic ratio) and constant brake pressure could be applied to achieve different operating strategies of the refrigerator.

Despite the above two methods, another significant method known as the constant rotating speed was newly adopted in the model. In this way, the brake pressure of turboexpander could stay the same in the cooling process for stability, and the expander inlet pressure was adjusted to keep rotating speed constant in the cooling process. This method was usually used to give full play to the ultimate capacity of bearings, especially for the gas bearings. Furthermore, the constant rotating speed together with constant brake pressure means the constant brake work. That is, the expansion work and brake work are both fixed. When the turboexpander uses a motor as brake, the rotating speed is constant in the working process and the brake power also remains the same. Thus, this method can be applied to simulate the expansion and brake characteristics when a motor is employed as a brake. Therefore, the operating strategy of the turboexpander running under constant rotating speed is quite meaningful and important.

As shown in Fig. 10, for a given rotating speed, the brake power could be calculated directly when the brake pressure is certain, and then the expansion work is got. On the other hand, based on the rotating speed and an assumed expansion ratio, the characteristic ratio and efficiency of the expander could be obtained through performance curves. Thus, another expansion work is obtained. Comparing two expansion works, we can reduce or raise the expansion ratio until the problem converges. Then the required expander operation parameters are obtained.

After improved, the matching model was applied to analyze the transient cooling performance of the cryogenic part. Through the dynamic matching model, the expander thermal performance under different control strategies of the refrigerator could be determined.

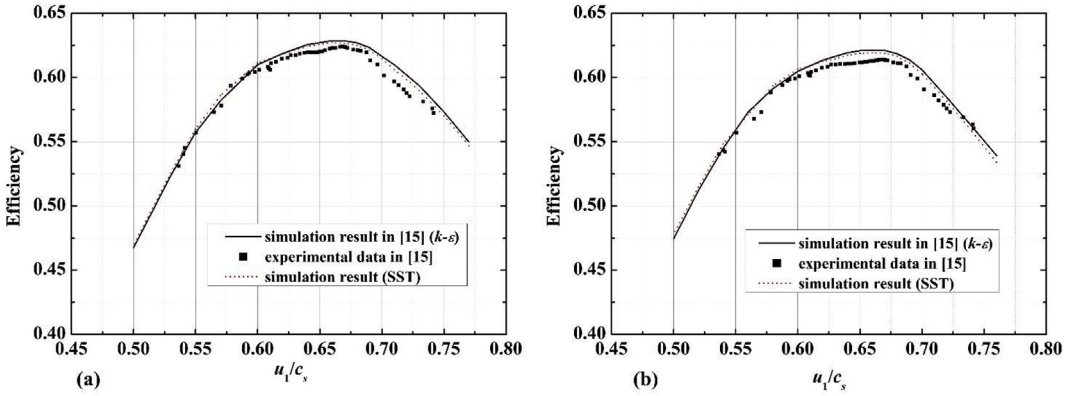

Fig. 9. Performance curves at different expansion ratios (a) $\varepsilon_E = 4.55$; (b) $\varepsilon_E = 5.13$.

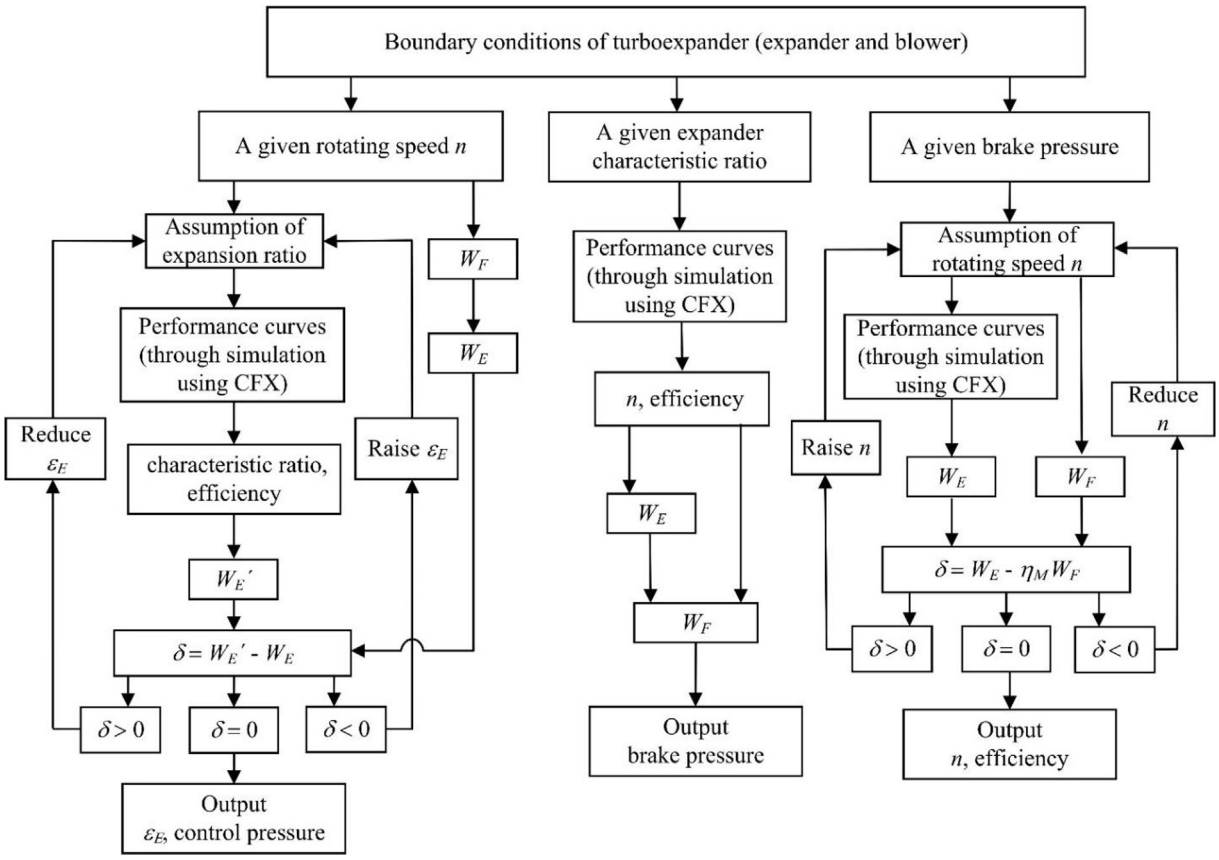

Fig. 10. Flowchart of the dynamic matching model.

3.3. Establishment of the transient cooling model

After developing models of the regenerator and expander, there exists a key factor that an effective method is required to connect the dynamic matching characteristics of turboexpander and the transient heat transfer characteristics of regenerator. In view of the shortcomings of existing researches and based on the cooling characteristics of the regenerator and turboexpander, we can describe the transient heat transfer process of the refrigerator using dual non-steady time steps. When the expander inlet temperature changes little, its outlet temperature is assumed to be constant. The total computation time is t_t, and the 1st time step is Δt. In each time step of Δt, the cold side inlet temperature of regenerator is the same as the expander outlet temperature, and the transient convection heat transfer occurs between the cold and hot fluid in the regenerator. With Δt as the total time, $\Delta \tau$ is divided as the 2nd time step. The transient convection heat transfer is calculated out by $\Delta \tau$ in Δt. Through transient calculations, the hot side outlet temperature of regenerator is obtained at the end of Δt, which means the expander inlet temperature is obtained. Thus, the expander outlet temperature can be calculated according to the matching model. Then the expander outlet temperature is treated as the inlet temperature of the cold fluid in the next time layer. The transient state in the next time layer of Δt is calculated. Repeating this until the calculation is terminated, the transient cooling characteristics are obtained. The flow chart of the calculated method is shown in Fig. 11.

Parameters that connect the regenerator and expander are the expander inlet and outlet ones, as shown in Eqs. (28) and (29).

$$T_{0E}^{k} = T_{h,n}^{k-1,m}, \quad T_{c,n}^{k,j} = T_{2E}^{k} \tag{28}$$

$$p_{0E}^{k} = p_{h,n}^{k-1,m}, \quad p_{c,n}^{k,j} = p_{2E}^{k} \tag{29}$$

where $j = 1, \ldots, m$; $k = 2, \ldots, p$.

In the refrigerator, because the flow area of regenerator is large and the expander is equipped with nozzles, the mass flow rate is determined by the boundary parameters of turboexpander.

$$m^{k} = m_{E}^{k} \tag{30}$$

where m^k is the mass flow rate of regenerator ($kg \cdot s^{-1}$); m_E^k is the mass flow rate of expander ($kg \cdot s^{-1}$); $k = 1, \ldots, p$.

Since the expander outlet pressure, which is slightly bigger than the ambient pressure, varies little in the cooling process, the mass flow rate mainly depends on the expander inlet parameters. As discussed above, the mass flow rate is regarded as constant in the 1st time step. The mass flow rate m_E is calculated using the expander inlet pressure and temperature [15,30].

3.4. Validation and calculation scheme of the cooling model

3.4.1. Experimental validation method

To verify the cooling model, several tests were conducted to compare with the calculation. The operation parameters of the tests were listed in Table 3 [15]. The cooling characteristics of refrigerator may change with the control strategy of the expander. With the

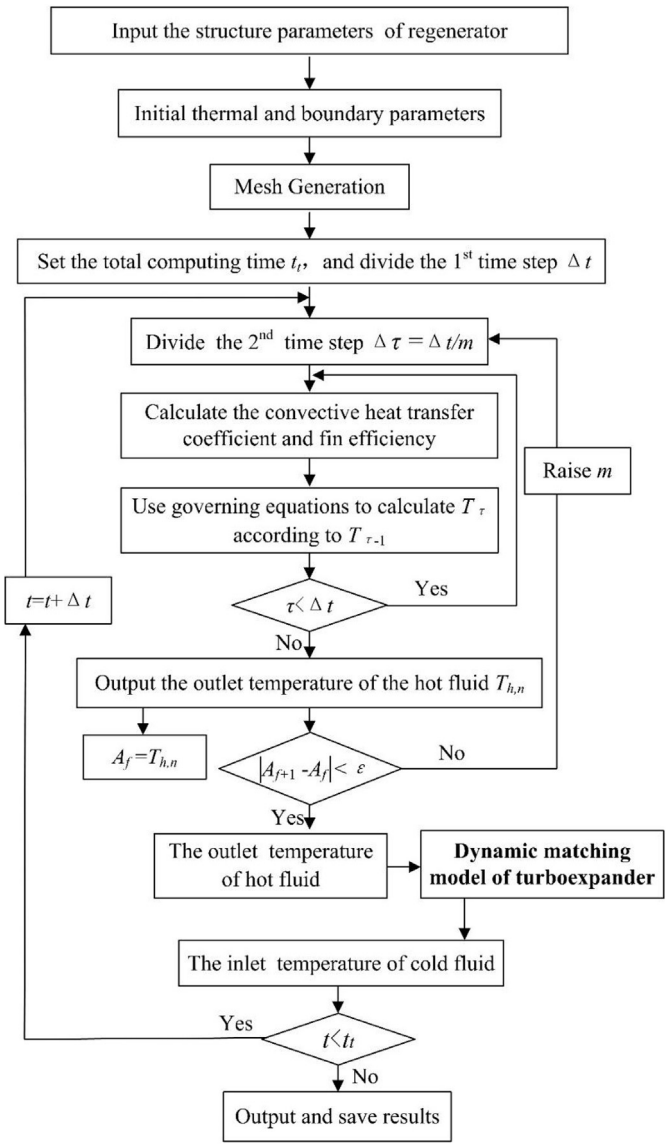

Fig. 11. Flowchart of the cooling model.

feed back control, the expander can operate under certain characteristic ratio (e.g. the optimal characteristic ratio) through regulating the brake pressure. With the constant brake pressure, the inlet pressure of the brake blower is fixed and the expander characteristic ratio varies in the cooling process. In the test, the local atmospheric pressure was 0.096 MPa. The matching model was analyzed in test 1 and test 2 in Ref. [15], and the experimental data of cooling process could be applied directly. Test 3 was repeated and improved to evaluate the cooling performance after regulation. Each experimental value was mean of three replicates, and the standard deviation was also presented.

Since the validity of the matching model had been verified by experiment [15], it was inserted into the transient cooling model directly. Then the cooling performance could be simulated through the model and compared with the experimental data. In tests 1 and 2, the refrigerator was operated under different expansion ratios, but both with the feed back control of optimal expander characteristic ratio. In test 3, the refrigerator was operated under constant brake pressure of turboexpander firstly and then the turboexpander was regulated to test the cooling performance under different expander efficiencies.

3.4.2. Theoretical validation method

The target parameter T_m reflects the final result of the transient process. It can also be obtained according to Fig. 1 (b) and Eq (2). Variations of T_m with the compressor pressure ratio and efficiency, expander efficiency, regenerator effectiveness, relative pressure drop, and ΔT_1, were then calculated. They were applied to complete validations and provide some theoretical corroborations for the transient cooling model.

3.4.3. Calculation scheme and operating strategies

To clarify the refrigerator transient characteristics, calculations should be carried out under different conditions. For a certain refrigerator, the performance of regenerator mainly depends on its boundary conditions and couldn't be changed actively. But the turboexpander could run with different control schemes through regulation. Thus, calculations were conducted under varied structure parameters of the regenerator, thermal performances of the expander and operation methods of the refrigerator.

The cutting length is an important factor of the regenerator, which influences both the convective heat transfer coefficient and pressure drop. For a turboexpander equipped with gas bearing, the starting pressure might be lower or higher than the operating pressure [5,16]. Therefore, the refrigerator might start with different expander inlet pressures. The starting pressure might be lower or higher than the operating pressure. A greater starting pressure usually means a larger startup shock and more energy costs. The operating strategy could be achieved by regulating inlet pressures of expander. Under the same expansion ratio, the refrigerator has different cooling performances with varied expander efficiencies. This operation strategy could also present the influence of expander efficiency on the ultimate refrigerating temperature, which can be achieved by changing the rotating speed. When a turboexpander works under a fixed rotating speed, the expansion work is constant and the expander inlet pressure should be regulated with the temperature. Even though at the same rotating speed, different expansion works might result in varied expansion and transient cooling performances. Variations of the rotating speed and expansion work could be obtained through regulating operation parameters of the expander and brake blower. Thus, calculations could be carried out under different cutting lengths of the regenerator, starting modes of the turboexpander, expander efficiencies, rotating speeds and expansion works. It could help formulating the effective control strategy and operation scheme of refrigerator. All the calculations were based on the environmental temperature and pressure of 300.0 K and 0.110 MPa.

Table 3
The operation parameters of test [15].

Test	Expander inlet pressure (MPa)	Regenerator inlet temperature (K)	Expander outlet pressure (MPa)	Control strategy of expander
1	0.499–0.502	293.2–294.3	0.108	feed back control
2	0.583–0.588	298.2–299.7	0.110	feed back control
3	0.499–0.503	293.7–296.5	0.108	constant brake pressure

3.5. Process optimization

To optimize the refrigerator performance at the steady state, the COP can be used as the target parameter to minimize the energy requirement and maximize the cold quantity. The exergy analysis can be applied to reduce exergy loss and find out the potential component for improvements. It could also provide relevant theoretical verifications for the transient cooling model. The exergy loss expressions of components were listed in Table 4. The exergy losses may be calculated and analyzed at the specified parameters of $T_a = 300$ K, $T_0 = 190$ K, $\varepsilon_C = 4.0$, $\eta_C = 0.75$, $\eta_E = 0.75$, $\eta_R = 0.85$, $\Delta T_1 = 0$ and $\Delta\varepsilon = 0.02$.

While for a practical refrigerator, the transient cooling model could be used to optimize components and the operation scheme. For example, the energy consumption and economic cost could be reduced through shortening the cooling process or decreasing in the total compression power, which could be simulated through the transient model. The heat regenerator sizing could be optimized to achieve low economic costs. For purposes of optimization, the mass flow rate could be specified. The work done per unit of cold production and the cooling down time formed the objective function:

$$f(x) = \min \int w_C dt = f(w_C, t_d) \tag{31}$$

where w_c is the compression work per unit, and t_d is the cooling time.

For the heat regenerator, accurate equipment sizing, specific structure parameter, proper pressure and flow rate specifications are necessary for simulation. By using the transient model, total surface area, layer configurations, and zone configuration as shown in Fig. 3 and Table 2, can be obtained under certain objective heat transfer and flow resistance characteristics. When calculating the surface area and volume, economic analysis for the regenerator is conducted and provides the basis for manufacturing. It influences the width and length of the heat regenerator. Combing the transient model and the objective function (31), the sizing and economic costs of the heat regenerator could be optimized.

Table 4
Exergy loss expressions for different components.

Equipment	Exergy loss equations
Compressor	$\Delta E_{xC} = E_1 - E_2 + W_C$
After cooler	$\Delta E_{xA} = E_2 - E_3$
Heat regenerator	$\Delta E_{xR} = E_3 + E_6 - E_4 - E_7$
Turboexpander	$\Delta E_{xT} = E_4 - E_5$
Cold load	$E_{xL} = E_5 - E_6 - E_{q_0}$
Valve and pipes	$E_{xV} = H_{in} - H_{out} - T_a(S_{in} - S_{out})$

4. Result and discussion

4.1. Verification of the cooling model

4.1.1. Experimental verification

The calculated and experimental data under two operation conditions were illustrated in Fig. 12. The calculated results agreed well with the experimental data under both conditions. In test 1 and test 2, the differences between theoretical and experimental ultimate refrigerating temperatures were 6.7 K and 2.8 K, and the relative deviations were 6.5% and 2.8%. The times it took to reach the lowest temperature were 116 and 98 min in the two tests, as compared to 108 and 96 min in the calculations. With the two time steps applied, the calculated results were precise when calculating the long time cooling, which also verified the previous transient analysis.

As shown in Fig. 13, the refrigerator was operated under constant brake pressure of turboexpander in the first 126 min. The calculated and experimental data also agreed well. While compared with test 1, the cooling speed was lower and ultimate refrigerating temperature was higher, which was due to the control strategy. With this control strategy, the characteristic ratio of turboexpander varied during the cooling process and the turboexpander efficiency was always lower than the optimal value [15].

A phenomenon that should be specially mentioned was also shown in Fig. 13. The temperature drops leveled off after 116 min, but there was a sudden decrease at about the 128th min. At this time, the brake pressure of turboexpander was regulated. With the regulation, the expander characteristic ratio changed and the expander efficiency increased from 0.571 to 0.602. Thus, the refrigerator was able to cool down further. After about 16 min, a new balance was established, and the ultimate refrigerating temperature decreased from 113.1 K to 109.3 K. This verified the conclusion that the brake pressure had a great influence on the expander efficiency [15,16]. It also proved the transient analysis in section 2.3.

As shown in the above comparisons, there were deviations between experimental and simulated results. There might be two primary reasons. First, the test results had some uncertainties. Second, the calculated model of refrigerator was based on the transient model of regenerator and the matching model of turboexpander, both of which had inevitable errors with the actual experiment. Whereas, the maximum relative deviation of ultimate refrigerating temperature was less than 6.5%, which showed that the calculation was satisfied with the actual needs.

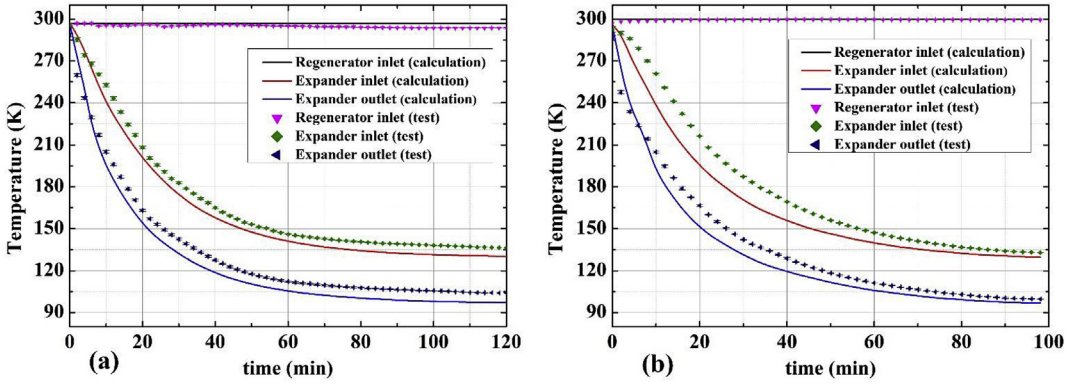

Fig. 12. Validation of the cooling model (a) test 1; (b) test 2.

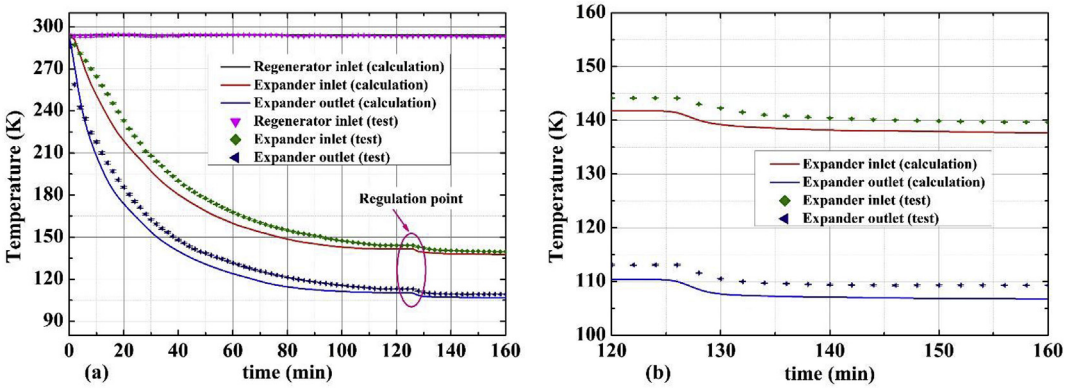

Fig. 13. Cooling performance under constant brake pressure with (a) cooling process; (b) cooling characteristics after regulation.

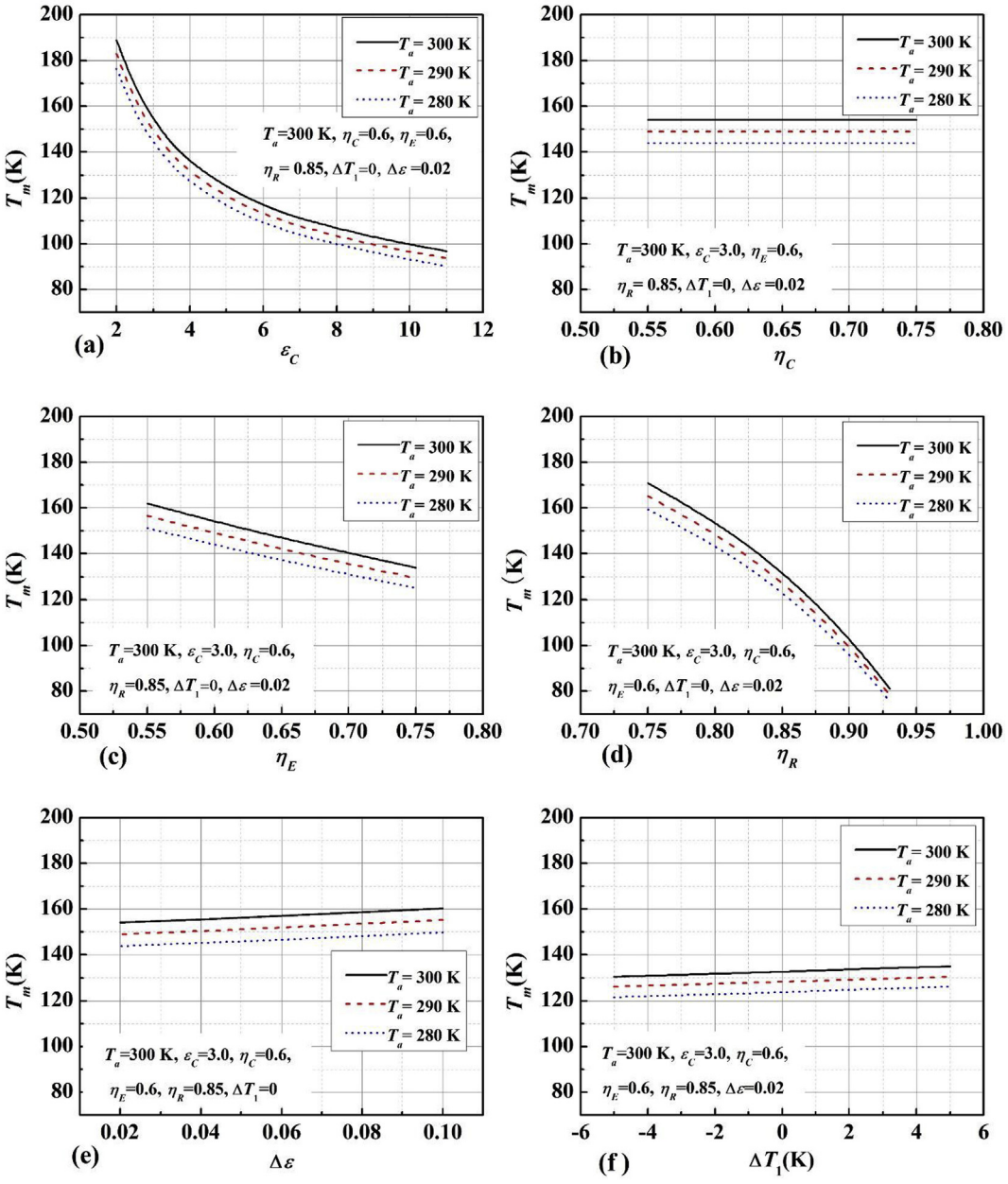

Fig. 14. Variations of T_m with the component performances.

4.1.2. Theoretical verification

The impact of component performances on the refrigerating temperature is presented in Fig. 14. T_m decreased with increasing pressure ratio and the downtrend became slower. As shown in Fig. 14 (b), T_m was not directly affected by compressor efficiency. As shown in Fig. 14 (c), T_m decreased with the increase of expander efficiency nearly linearly, and the variation tendency basically didn't vary with T_a. T_m decreased by 4.6 K, when η_E decreased by 0.03, as compared to 3.7 K in the transient calculation in Fig. 13. It proved that the ultimate refrigerating temperature was limited by the expander efficiency, as discussed in section 4.1.1. As shown in Fig. 14 (d), T_m decreased with the increase of regenerator effectiveness, and the downward trend was getting faster. With the increase of regenerator effectiveness, influence of T_a on T_m became small. As shown in Fig. 14 (e) and (f), T_m increased with the relative pressure drop and ΔT_1 under certain T_a. T_m decreased by 2.2 K, when ΔT_1 decreased by 5.0 K. In a word, the most significant factor impacting the ultimate refrigerating temperature was the regenerator effectiveness, followed by the expander efficiency and compressor pressure ratio. It also verified constrains of the ultimate refrigerating temperature as derived from the transient cooling model.

It can be concluded from Fig. 13 that influences of the expander and regenerator on the ultimate refrigerating temperature were crucial for a cryogenic refrigerator. The calculations verified the analysis in sections 2.2 and 2.3 that the expander and regenerator might affect the refrigerator cryogenic performance greatly. Additionally, the transient cooling model of the cryogenic part, including models of the regenerator and expander, was important for studying the whole refrigerator.

Table 5
Main component exergy losses.

Parameters	ΔE_{xC}	ΔE_{xA}	ΔE_{xR}	ΔE_{xT}	ΔE_{xL}	ΔE_{xV}	E_{q_0}
Exergy loss (%)	16.5	23.1	3.1	41.9	3.4	0.9	11.1

4.1.3. Exergy calculation

As shown in Table 5, the exergy efficiency of the refrigerator was 11.1%. The exergy losses in the compressor, after cooler, and turboexpander were large. Since the pressure ratio was great and the compression efficiency was limited, the compressors contributed great exergy losses in the process. The heat from the hot air was emptied and unused when the air was cooled in the after cooler. If the expansion work was consumed and constrained by the expander efficiency, the expander contributed the greatest exergy loss. It could be improved by high efficiency and energy recovery. Because the turboexpander belonged to the cryogenic part, it was plausible to choose it as the primary objective of the transient model.

4.2. Cooling performance under different cutting lengths of the regenerator

The transient cooling performance of the refrigerator under different regenerator cutting lengths were presented. As shown in Fig. 15 (a), with the cutting lengths of 5, 10 and 15 mm, the ultimate refrigerating temperatures reached 101.8, 103.8 and 104.4 K, respectively. Cooling tendencies under three conditions were nearly the same, so was the cooling rate, as shown in Fig. 15 (b). As shown in Fig. 15 (c), the shorter cutting length generated greater heat transfer coefficient and higher effectiveness, but also larger pressure loss. As shown in Fig. 15 (d), variations of the ultimate refrigerating temperature with the cutting length were presented. The change trend was nonlinear, and the cutting length should be chosen carefully. With a shorter cutting length, the turbulent flow

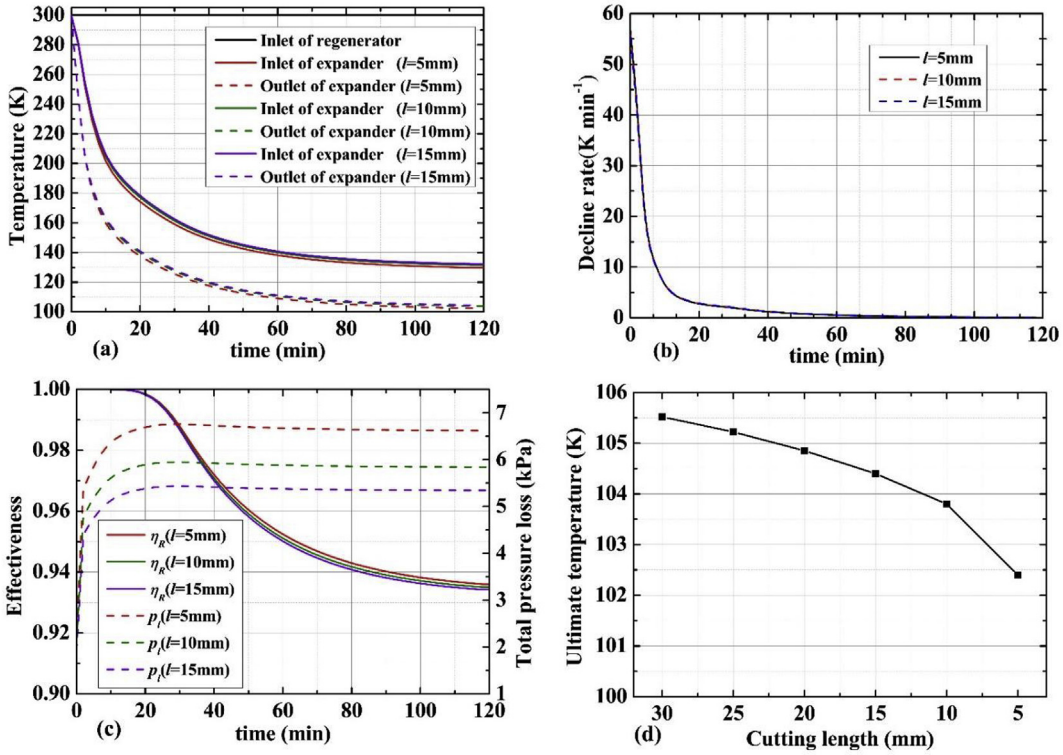

Fig. 15. Influence of cutting length at $\varepsilon_E = 4.54$ and $\eta_E = 0.6$ (a) cooling characteristics; (b) decline rate; (c) regenerator performance; (d) ultimate refrigerating temperature with the cutting length.

could be developed more sufficiently and thermal boundary layer can be reduced. That is, the heat transfer is enhanced and friction resistance increases. Therefore, a good balance should be obtained between the heat transfer and flow resistance. Also, the shorter cutting length may raise the manufacturing difficulty and economic costs.

Different from the expander which could be regulated under different working conditions, the regenerator is inherently determined by its structure parameters and influenced by boundary conditions to some degree. That is, the careful design and rigorous verification are essential for a regenerator. Also, good matching between the regenerator and expander is vital for the efficient operation of a refrigerator.

4.3. Influence of turboexpander starting modes on the cooling performance

As shown in Fig. 16, the transient cooling performance under different starting modes was illustrated. During the first 20 min, the expander inlet pressure varied linearly to 0.500 MPa with different paths. As shown in Fig. 16 (b), the higher expansion ratio in the starting period generated faster refrigerator cooling speed. When expansion ratios were close and consistent, the cooling characteristics were similar and the ultimate refrigerating temperatures were nearly the same. The reasons could be found in Fig. 16 (c) and (d). In the first several minutes, the higher expansion ratio resulted in the bigger decline rate. When the cooling went on, the decline rates were inverse under different conditions. That was because, higher expansion ratio resulted in lower expander outlet temperature. With the convective heat transfer in the regenerator, the lower expander inlet temperature accrued. The lower expander inlet temperature is responsible for the lower enthalpy drop. Thus, the inversion phenomenon occurred when the cooling went to a certain extent and the expander inlet temperature began to have a greater effect. It was the result of a combination of the expansion ratio, expansion characteristics and heat transfer characteristics in regenerator. A lower expander inlet pressure means a smaller pressure ratio and therefore a lower energy consumption. Thus, to start with a relatively smaller pressure in the beginning period might have a higher energy efficiency. Also, it is beneficial for the stability of the gas bearing turboexpander. A lower expansion ratio may result in lower rotating speed and smaller load capacity of gas bearing. Then, a feed back control could be applied to have the expander operating under high efficiency in the long-term cooling process. Total energy consumption decreased with the operating pressure of turboexpander, which was constrained by starting pressure of the gas bearing. Although the control system requires additional costs, the start and operation responses enable a form of energy saving and lower economic cost for a large-scale plant.

4.4. Influence of expander efficiency on the cooling performance

As shown in Fig. 17 (a), under certain value of expander efficiency, the ultimate temperature of the refrigerator was limited. The higher expander efficiency generated faster cooling speed and lower ultimate refrigerating temperature. When the expander efficiency increased, the refrigerator reached the ultimate refrigerating temperature relatively earlier. It can be seen from Fig. 17 (b) that, the regenerator effectiveness was nearly the same under different conditions after 30 min. As shown in Fig. 17 (c) and (d), the decline rates of expander outlet temperatures were presented. In the first several minutes, the higher the expander efficiency went the faster the decline rate. When the cooling went on, the decline rates under different conditions were nearly the same. That was because, the refrigerator was more affected by expander efficiency in the starting period of the cooling process. When the temperature

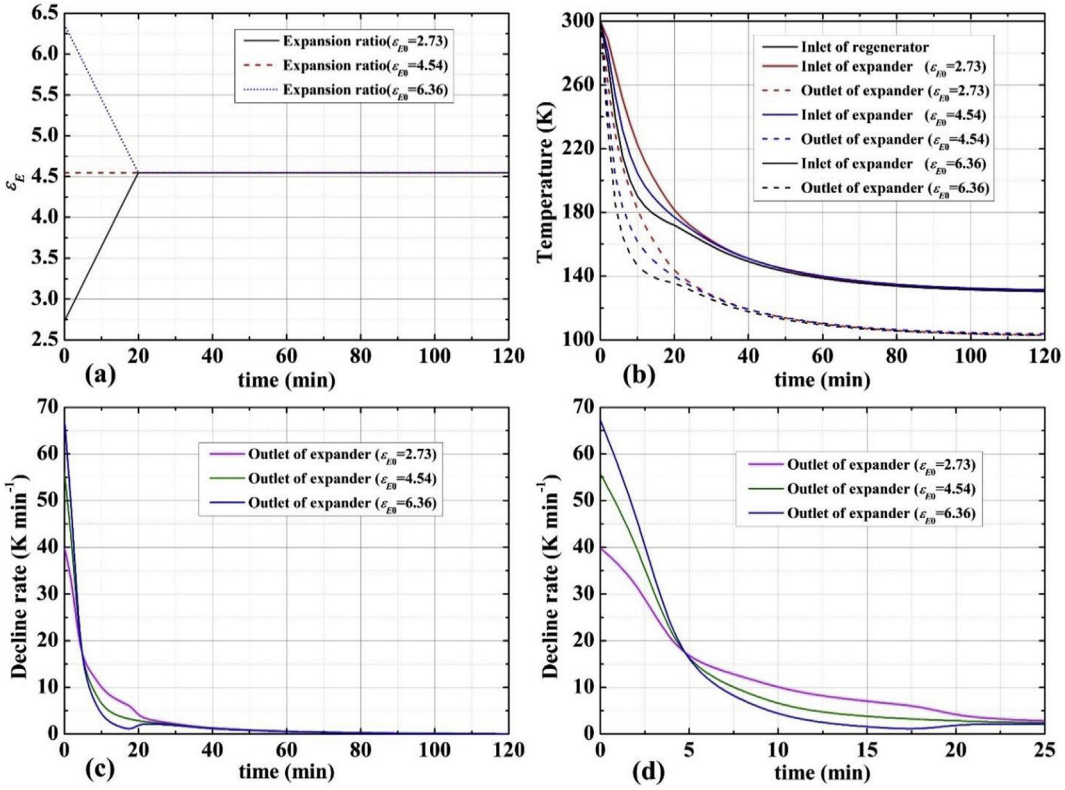

Fig. 16. Cooling characteristics under different starting modes at $\eta_E = 0.6$ (a) expansion ratio; (b) cooling process; (c) decline rate; (d) decline rate at the beginning of 25 min.

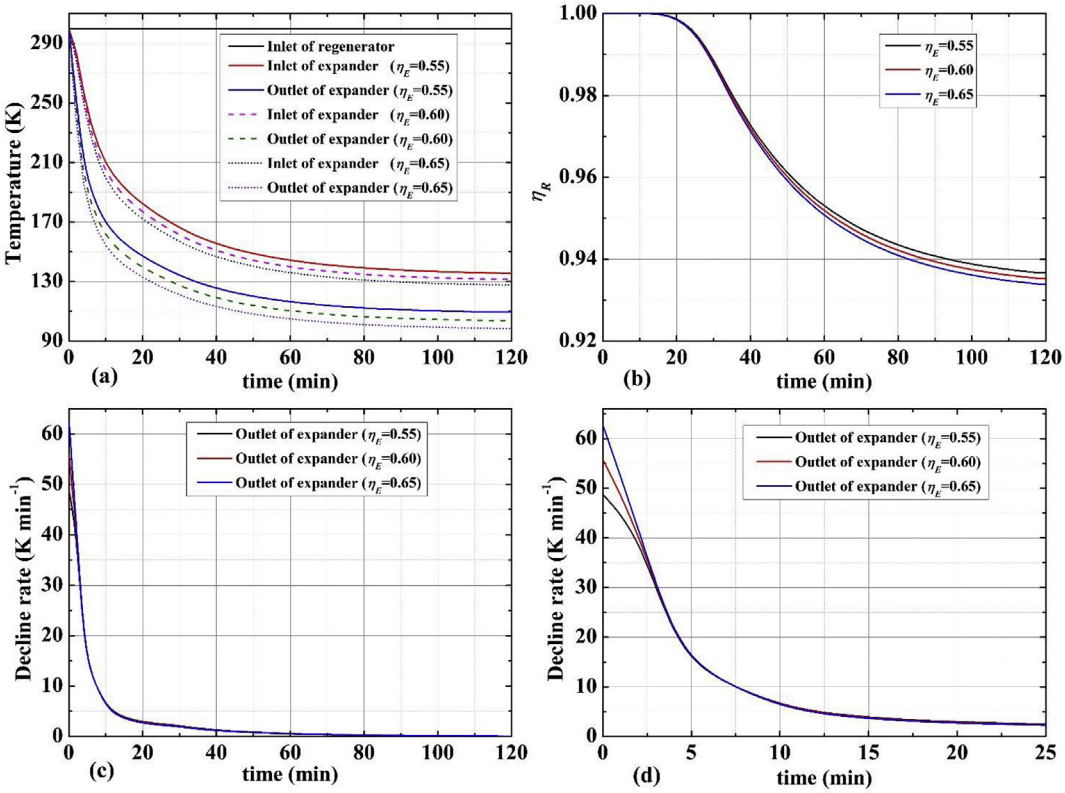

Fig. 17. Cooling characteristics under different expander efficiency at $\varepsilon_E = 4.54$ (a) cooling process; (b) regenerator effectiveness; (c) decline rate; (d) decline rate at the beginning.

decreased to some extent, the influence of regenerator effectiveness on the refrigerator became larger than that of the expander efficiency. Their joint effects brought changes of the cooling characteristics along with time. Although the decline rate became close later, the higher expander efficiency resulted in the lower refrigerating temperature finally. These also verified the conclusions in 4.1.2.

4.5. Cooling performance under constant rotating speed of turboexpander

As shown in Fig. 18, the refrigerator cooling performance with turboexpander rotating speed of 170k rpm was presented. Under different expansion works, the cooling characteristics were different. The ultimate refrigerating temperatures were 108.0, 111.1, and 108.9 K, respectively, under expansion works of 560, 610 and 660 W. That is, the bigger expansion work does not always mean the greater cooling ability of refrigerator. The reason can be found in Fig. 18 (b). Under different expansion works, the expansion ratio and expander efficiency had different variation tendencies. At the expansion work of 560 W, there existed a greater expansion ratio and a lower expander efficiency. The variations of expansion ratio and expander efficiency had inverse effects on the refrigerator, and they along with the regenerator leaded to a higher refrigerator efficiency ultimately. From a different angle, the expansion work reflects the cooling capacity of the expander but does not reflect the cooling temperature. The lower expansion work might be corresponding to a lower temperature, leading to a faster cooling speed.

As shown in Fig. 19, the refrigerator cooling performance with expander rotating speed of 200k rpm was presented. The ultimate refrigerating temperatures were 108.7, 106.6, and 104.7 K, respectively, under expansion works of 910, 990 and 1070 W. Under this

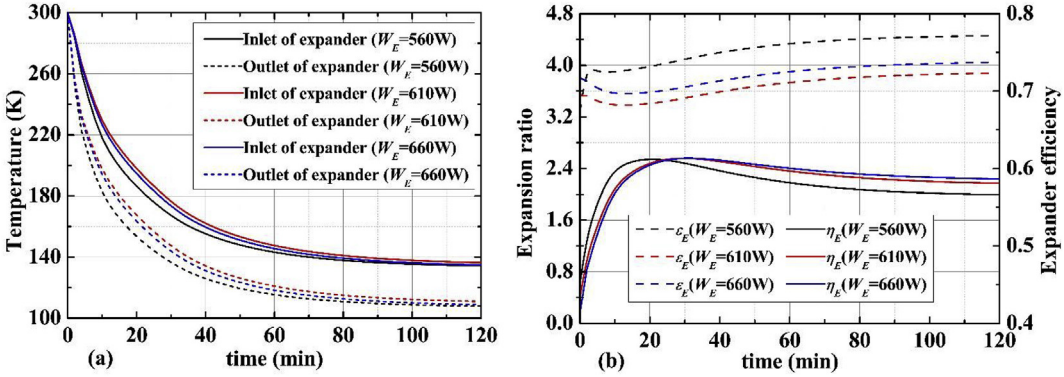

Fig. 18. Cooling characteristics at rotating speed of 170k rpm (a) cooling process; (b) expansion ratio and efficiency.

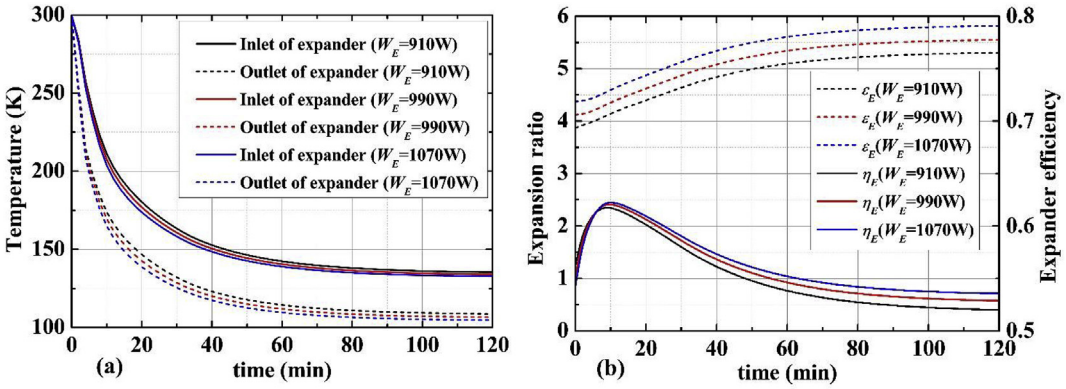

Fig. 19. Cooling characteristics at rotating speed of 200k rpm (a) cooling process; (b) expansion ratio and efficiency.

rotating speed, the expansion work and the refrigerator cooling ability had positive correlations. The reason was shown in Fig. 19 (b). Under different expansion works, the expansion ratio and expander efficiency had similar variation tendencies. The bigger the expansion work, the greater expansion ratio and expander efficiency were. The expansion work of 1070 W was corresponding to a greater expansion ratio and a higher expander efficiency, and thus leaded to a higher refrigerator efficiency.

It can be seen from Figs. 18 and 19 that, although both operated under constant rotating speed, the different change rules between refrigerating ability and expansion work came from the nonlinear expansion characteristics and the mutual interactions between the expander and regenerator. The expansion work W_E can be expressed in the following form [15,33]:

$$W_E = BCT_{0E}^{0.5} \tag{32}$$

where $B = A_{\min}\left(\frac{k_E}{k_E-1}\right)^{1.5}\left[R(n_Z-1)(2/n_Z+1)^{\frac{n_Z+1}{n_Z-1}}/Z_{0E}\right]^{0.5} p_{2E}$,
$C = (\varepsilon_E - {\varepsilon_E}^{1/k_E})\eta_E$.

In the present refrigerator, p_{2E} is nearly equal to the atmosphere one, and B can be recognized as constant. Then the expansion work is related to the expansion ratio, expander efficiency and expander inlet temperature. With the decrease of T_{0E}, C should be raised to keep the expansion work constant. That is, the change rule of the expansion ratio and expander efficiency must meet the demand that C increases with the decrease of T_{0E}. For example, whenε_E decreases, η_E has to arise. When $\varepsilon_E$increases, η_E could rise or fall, which is determined by the expansion characteristics and reflected on the performance curves. As shown in Fig. 18 (b), η_E increased with the decrease of ε_E at the beginning. Then η_E decreased with the increase of ε_E under different expansion works, but the variation tendencies were obviously different. As shown in Fig. 19, η_E decreased with the increase of ε_E, and the variation tendencies were similar. That is because, under different expansion ratios, variations of efficiency with characteristic ratio were somewhat different [15], as shown in Fig. 9. In addition, the change trend of T_{0E} is the result of the interactions between the expander and the regenerator. That is why there are differences between the rotating speeds of 170k rpm and 200k rpm. Therefore, to promote energy efficiency and reduce economic costs, a careful and accurate calculation is necessary when the operation method of constant rotating speed is applied.

The influence of parameters on the refrigerator cooling performance is non-linear and coupled together, which can be demonstrated through the transient model. Compared to the ordinary system, the transient model results in greater cold production with obviously lower energy consumptions and economic costs.

5. Conclusion

This paper focused on transient analysis of the cryogenic part in reverse Brayton air refrigerator, defined the ultimate refrigerating temperature T_m, and established the transient cooling model of the cryogenic part. The steady-state parameter analysis provided theoretical foundation based on T_m and exergy losses. The transient characteristics of regenerator was calculated through methods of numerical heat transfer and computational fluid dynamics. The dynamic matching model of turboexpander was improved by adopting a significant method known as the constant rotating speed. Using the newly proposed method of dual non-steady time steps to connect the regenerator and turboexpander, a transient cooling model was built and validated by tests. When the expander efficiency increased from 0.571 to 0.602 through regulation, T_m decreased from 113.1 K to 109.3 K.

With the regenerator cutting lengths of 5, 10 and 15 mm, T_m reached 101.8, 103.8 and 104.4 K, respectively, and the change trend was nonlinear. A relatively smaller pressure in the beginning period (e.g. during the first 20 min) may produce higher energy efficiency, which is also beneficial for the stability of the gas bearing turboexpander. The refrigerator was clearly affected by expander efficiency in the starting period. When the temperature decreased to some extent, the influence of regenerator effectiveness became large. T_m was 108.0, 111.1, and 108.9 K, respectively, under expansion works of 560, 610 and 660 W with rotating speed of 170k rpm but 108.7, 106.6, and 104.7 K, respectively, under expansion works of 910, 990 and 1070 W with rotating speed of 200k rpm. The transient model could provide a basis for the design and optimization of the cryogenic part in refrigerators. It can be used to evaluate the management and operation strategy of refrigerators and help to promote energy efficiency and reduce economic costs.

Acknowledgement

This project was supported by the National Natural Science Foundation of China (51506209), Fundamental Research Funds for the Central Universities and the Key Scientific Research Projects in Henan Colleges and Universities (18A470006).

Appendix A. Supplementary data

Supplementary data related to this article can be found at https://doi.org/10.1016/j.energy.2018.11.016.

References

[1] Flynn T. Cryogenic Engineering. Revised and Expanded. Colorado: CRC Press; 2004.
[2] Remeljej CW, Hoadley AFA. An exergy analysis of small-scale liquefied natural gas (LNG) liquefaction processes. Energy 2006;31:2005–19.
[3] Nicholas J, Darell Z, Walter S, Francis D. A mechanical cryogenic cooler for the Hubble Space Telescope. In: Presented at the 39th space congress, FL, USA; 2002.
[4] Deserranno D, Zagarola M, Li X, Mustafi S. Optimization of a Brayton cryocooler for ZBO liquid hydrogen storage in space. Cryogenics 2014;64:172–81.
[5] Hou Y, Zhao HL, Chen CZ, Xiong LY. Development in reverse Brayton refrigerator in China. Cryogenics 2006;46:403–7.
[6] Lechon Y, Cabal H, Varela M, Saez R, Eherer C, Baumann M, et al. A global energy model with fusion. Fusion Eng Des 2005;75:1141–4.
[7] Hiraia H, Suzukia Y, Hirokawaa M, Kobayashia H, Kamiokaa Y, Iwakuma M, et al. Development of a turbine refrigerator for high temperature superconductor applications. Physica C 2009;469:1857–61.
[8] Spence SWT, Doran WJ, Artt DW. Design, construction and testing of an air-cycle refrigeration system for road transport. Int J Refrig 2004;27:503–10.
[9] Ahmadi MH, Ahmadi MA, Pourfayaz F, Bidi M. Thermodynamic analysis and optimization for an irreversible heat pump working on reversed Brayton cycle. Energy Convers Manag 2016;110:260–7.
[10] Biglia A, Comba L, Fabrizio E, Gay P, Mannini A, Mussinatto A, Aimonino RD. Reversed Brayton cycle for food freezing at very low temperatures: energy performance and optimisation. Int J Refrig 2017;81:82–95.
[11] Kim D, Creary A, Chang SS, Kim JH. Mesoscale foil gas bearings for palm-sized turbomachinery: design, manufacturing, and modeling. J Eng Gas Turbines Power 2009;131(4):042502.
[12] Hirai H, Hirokawa M, Yoshida S, Nara N, Ozaki S, Hayashi H. Neon turbo-Brayton cycle refrigerator for HTS power machines. AIP Conf Proc 2012;1434(1):1672–9.
[13] Davis F, Agahi R, Wu R. Full load, full speed test of turboexpander-compressor with active magnetic bearings. In: Proc. 35th turbomachinery symposium; 2006. p. 81–8.
[14] Dolan FX, Swift WL, Tomlinson LBJ, et al. A single stage reverse Brayton cryocooler: performance and endurance tests on the Engineering model//cryocoolers 9. Springer US; 1997. p. 465–74.
[15] Hou Y, Yang SJ, Chen XY, Chen ST, Lai TW. Study on the matching performance of a low temperature reverse Brayton air refrigerator. Energy Convers Manag 2015;89:339–48.
[16] Yang SJ, Chen ST, Chen XY, Zhang XQ, Hou Y. Study on the coupling performance of a turboexpander compressor applied in cryogenic reverse Brayton air refrigerator. Energy Convers Manag 2016;122:386–99.
[17] Xia K, Yao YX, Yang JH, Wang K, Chen CZ. Study on the transient cooling characteristics of air refrigerator. Cryogenics (in Chinese) 2003;134(4):25–32.
[18] Cai JW, Sun W, Li B, Li T, Hou Y. Study on the dynamic cooling performance of a -150 °C reverse Brayton cycle air cryocooler. J Xi'an Jiaotong Univ 2013;47(3):60–3.
[19] Ahmadi MH, Ahmadi MA. Thermodynamic analysis and optimization of an irreversible Ericsson cryogenic refrigerator cycle. Energy Convers Manag 2015;89:147–55.
[20] Ahmadi MH, Ahmadi MA, Mohammadi AH, Feidt M, Pourkiaei SM. Multi-objective optimization of an irreversible Stirling cryogenic refrigerator cycle. Energy Convers Manag 2014;82:351–60.
[21] Ahmadi MH, Ahmadi MA, Mehdi M, Hosseinzade H, Feidt M. Thermodynamic and thermo-economic analysis and optimization of performance of irreversible four-temperature-level absorption refrigeration. Energy Convers Manag 2014;88:1051–9.
[22] Ahmadi MH, Ahmadi Mohammad-Ali, Feidt M. Thermodynamic analysis and evolutionary algorithm based on multi-objective optimization of performance for irreversible four-temperature-level refrigeration. Mech Ind 2015;16(2):207.
[23] Zhan Y, Wang J, Wang W, Wang R. Dynamic simulation of a single nitrogen expansion cycle for natural gas liquefaction under refrigerant inventory operation. Appl Therm Eng 2018;128:747–61.
[24] Fazlollahi F, Bown A, Ebrahimzadeh E, Baxter LL. Design and analysis of the natural gas liquefaction optimization process-Energy Storage of Cryogenic Carbon Capture (CCC-ES). Energy 2015;90:244–57.
[25] Fazlollahi F, Bown A, Ebrahimzadeh E, Baxter LL. Transient natural gas liquefaction and its application to CCC-ES (energy storage with cryogenic carbon capture™). Energy 2016;103:369–84.
[26] Fazlollahi F, Bown A, Saeidi S, Ebrahimzadeh E, Baxter LL. Transient natural gas liquefaction process comparison-dynamic heat exchanger under transient changes in flow. Appl Therm Eng 2016;109:775–88.
[27] He TB, Ju YL. Dynamic simulation of mixed refrigerant process for small-scale LNG plant in skid mount packages. Energy 2016;97:350–8.
[28] McCormick JA, Nellis GF, Swift WL, Sixsmith H, Reilly J. Design and test of low capacity reverse Brayton cryocooler for refrigeration at 35K and 60K[M]//Cryocoolers 10. Boston, MA: Springer; 2002. p. 421–9.
[29] Shin Y, Lee YP. Design of a boil-off natural gas reliquefication control system for LNG carriers. Appl Energy 2009;86:37–44.
[30] Bradu B, Gayet P, Niculescu SI. A process and control simulator for large scale cryogenic plants. Control Eng Pract 2009;17:1388–97.
[31] Averous D, Hammadi K, Pingaud H, Joulia X, Guittard P. Dynamic simulation of brazed plate-fin heat exchangers. Comput Chem Eng 1999;23(99):S447–50.
[32] Joshi MH. Heat transfer and friction in the offset strip-fin heat exchanger. Int J Heat Mass Tran 1987;30(1):69–84.
[33] Whitfield A, Baines NC. Design of radial turbomachines. Longman Scientific & Technical; 1990. ISBN 0-470-21667-0.
[34] Kim JH, Choi JH, Husain A, Kim KY. Multi-objective optimization of a centrifugal compressor impeller through evolutionary algorithms. P I Mech Eng A-J Pow 2010;224(5):711–21.